JACS
JOURNAL OF THE AMERICAN CHEMICAL SOCIETY

ARTICLE

pubs.acs.org/JACS

Evidence for the Pairwise Disposition of Grafting Sites on Highly Dehydroxylated Silicas via Their Reactions with $Ga(CH_3)_3$

Samuel D. Fleischman[†] and Susannah L. Scott[*,†,‡]

[†]Department of Chemistry & Biochemistry, University of California, Santa Barbara, California 93106-9510, United States
[‡]Department of Chemical Engineering, University of California, Santa Barbara, California 93106-5080, United States

Supporting Information

ABSTRACT:

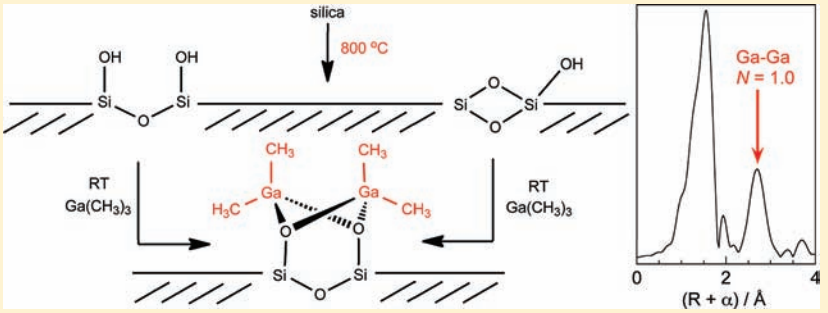

Molecules encountering silica interfaces interact primarily with the hydroxyl groups that terminate the bulk structure. When the nominal surface density is very low, these "silanols" are presumed to be isolated. Nevertheless, silicas that are highly dehydroxylated by pretreatment at 800 °C react with $Ga(CH_3)_3$ at room temperature to give primarily disilanolate-bridged digallium sites, $[(CH_3)_2Ga(\mu\text{-}OSi\equiv)]_2$. The EXAFS at the Ga K-edge shows a prominent Ga−Ga scattering path, regardless of whether an excess or a limiting amount of $Ga(CH_3)_3$ is used. Some dimers are formed by the concerted reaction of $Ga(CH_3)_3$ with an "isolated" silanol and an adjacent siloxane bond. These grafting sites are proposed to be hydroxyl-substituted 2-rings, formed by condensation within a vicinal Q^2-Q^3 pair. Other dimers are formed by reaction of $Ga(CH_3)_3$ with vicinal Q^3-Q^3 pairs which have not condensed, even at 800 °C. In a computational model for the dimer sites, the O−O distance is <2.6 Å, which is far shorter than the calculated mean interhydroxyl separation for the thermally treated silicas (12.2 Å). This highly nonrandom distribution of surface silanols, in combination with the coupled reaction of "isolated" silanols and strained siloxane bonds, accounts for the preferential formation of grafted site pairs rather than isolated grafted sites when silica surfaces are chemically modified.

The hydroxyl-terminated surface of silica is a component of many important interfaces. For example, it is present in silicon-based microelectronics,[1,2] and its selective adsorption properties are the basis for many chromatographic separations.[3,4] Amorphous silica glasses are used in fiber optics, where mechanical fatigue is attributed to stress corrosion initiated at surface defects.[5] Silica can be incorporated into organic polymers to give organic−inorganic nanocomposites; interactions between the hydroxyl-terminated silica surface and the polymer in the interfacial region can enhance the thermal and mechanical properties of the polymer.[6] When nanostructured thin films are grown by metal−organic atomic layer deposition (ALD) or chemical vapor deposition (MOCVD) on Si substrates, the metal-containing compounds initially become attached to the substrate via their reactions with the hydroxyl groups of the oxidized (i.e., silica) surface layer.[7] The finely divided silicas that are widely used as catalyst supports anchor metal complexes via their reactions with surface hydroxyls, thereby stabilizing coordinatively unsaturated active sites.[8−10] Two general strategies used in such covalent anchoring are shown in Scheme 1. *Grafting* involves ligand protonolysis by surface hydroxyl groups with concurrent formation of metal−silanolate bonds, while *tethering* requires that the hydroxyl groups react with a ligand-based functional group, such as an alkoxy- or chlorosilane.[11]

Altering the physisorbed water and/or the hydroxyl (reacted water) content of a silica can dramatically change its mechanical stability[5] and, on the surface, its reactivity toward small molecules.[12] Thermal pretreatment of the silica supports used in catalysis reduces their surface hydroxyl population, which controls the density of anchored sites and is believed to limit bimolecular deactivation reactions.[8−10] The hydroxyl groups of silica have low or no mobility at moderate temperatures (≤450 °C).[13−15] Consequently, the hydroxyl population in high surface area silicas decreases slowly as the temperature increases, and it is still appreciable just prior to the onset of sintering (ca. 1200 °C).[16]

Received: October 2, 2010
Published: February 22, 2011

Scheme 1. Immobilization Strategies on Partially Dehydroxylated Silica Surfaces: (a) *Grafting*, via Protonolysis of a Metal−Ligand Bond, and (b) *Tethering*, via Protonolysis of a Remote Silyl Substituent (X = Cl, OR)

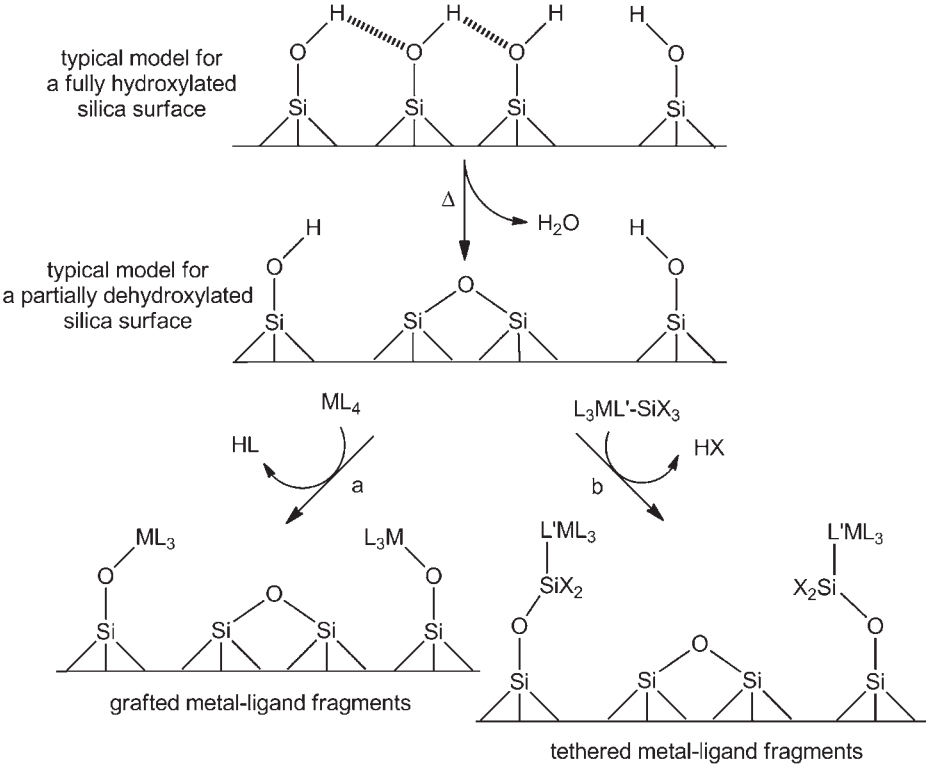

The spatial distribution of the hydroxyl groups on the surfaces of amorphous silicas is usually inferred from the broadening and red-shifting of the ν(SiO−H) band in the infrared spectrum.[12] A wide range of fully hydroxylated, amorphous silicas have been reported to have surface hydroxyl densities of ca. 4.9 nm^{-2},[17] regardless of the synthesis method, and their IR spectra confirm the presence of extensive hydrogen-bonding.[12] Figure 1 shows how such interactions are greatly diminished by heating to 500 °C, due to condensation of adjacent hydroxyl groups with elimination of water. The resulting hydroxyl density, assuming all remaining OH groups are located on the surface, is ca. 1.4 nm^{-2},[17,18] corresponding to a mean interhydroxyl distance of 8.4 Å.[19] In the absence of other information about their distribution, these silanols have long been presumed to be "isolated", at least from the perspective of a small-molecule adsorbate.[12] We were therefore surprised to find that the hydroxyl sites of a high surface area silica, pretreated at 500 °C, reacted with $Ga(CH_3)_3$ in a pairwise manner,[20] eq 1,

$$2\ \equiv\!SiOH + 2Ga(CH_3)_3 \rightarrow [(CH_3)_2Ga(\mu\text{-}OSi\equiv)]_2 + 2CH_4 \quad (1)$$

where ≡Si represents a surface silicon atom attached to the silica framework via three siloxane bonds. The formation of these disilanolate-bridged digallium sites appears to be analogous to the reaction of $Ga(CH_3)_3$ with simple, molecular silanols. For example, protonolysis by $(C_6H_5)_3SiOH$ yields $[(CH_3)_2Ga(\mu\text{-}OSi(C_6H_5)_3)]_2$.[20,21]

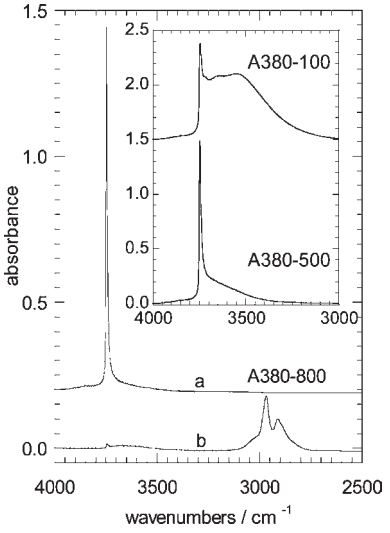

Figure 1. *In situ* transmission IR spectra of a self-supporting disk of A380 silica (a) after partial dehydroxylation *in vacuo* at 800 °C (A380-800) and (b) after the gas−solid reaction with excess $Ga(CH_3)_3$ at room temperature, followed by desorption of volatiles at the same temperature. Spectra are normalized to the intensity of the silica mode at 1875 cm^{-1} and are offset vertically for clarity. Inset: IR spectra of A380 silica disks partially dehydroxylated at 100 and 500 °C, showing the evolution of the hydrogen-bonding interactions of the surface hydroxyls with increasing dehydroxylation temperature.

It has been proposed that the probability of grafting reactions involving more than one hydroxyl site may be reduced or even eliminated by effecting very extensive dehydroxylation of silica,

dx.doi.org/10.1021/ja108905p |*J. Am. Chem. Soc.* 2011, 133, 4847–4855

using temperatures even higher than 500 °C.[22,23] In contrast to the silanols, the siloxane bonds in silica are largely unreactive. However, silicas heated at temperatures above 600 °C also possess highly strained siloxane bonds that may participate in anchoring reactions.[18,24,25] In order to explore whether site isolation of grafted metal complexes on silica can be achieved at nominal surface hydroxyl densities significantly lower than 1.4 nm^{-2}, we explored the reaction of $Ga(CH_3)_3$ with two highly dehydroxylated silicas, a nonporous, fumed silica (Aerosil 380, 383 m^2/g) and a mesoporous, precipitated silica (Sylopol 952, 300 m^2/g), after pretreating each *in vacuo* at 800 °C. The hydroxyl content of a particular silica depends on its preparation, age, and thermal history.[12,26] The values for the Aerosil and the Sylopol, after heating at 800 °C, are 0.43 and 0.45 mmol OH/g, respectively. They correspond to 0.68 OH/nm^2 (A380-800) and 0.71 OH/nm^2 (S952-800), for a mean interhydroxyl distance of ca. 12 Å on both silicas.

RESULTS AND DISCUSSION

Reaction of A380-800 Silica with Excess $Ga(CH_3)_3$. The IR spectrum of A380-800 shows a single, symmetrical O−H stretching mode at 3747 cm^{-1}, with no low-energy shoulder due to hydrogen-bonding interactions (Figure 1a). The reaction between A380-800 and excess $Ga(CH_3)_3$ vapor at room temperature yielded 0.43 ± 0.06 mmol of CH_4/g of SiO_2, confirming that the hydroxyl groups of the silica are the sole source of labile protons participating in the grafting reaction. Figure 1b shows that these hydroxyls are consumed essentially completely, while new IR bands associated with adsorbed methyl groups appear in the C−H stretching region (3100−2800 cm^{-1}).

Spatial Arrangement of the Grafted $Ga(CH_3)_2$ Fragments. The IR spectrum provides no information about the proximity of the anchored dimethylgallium sites; however, this relationship can be probed by X-ray absorption spectroscopy at the Ga K-edge. The intensity of the white-line at the absorption edge, shown in the Supporting Information (SI), Figure S1, is consistent with four-coordinate Ga, based on its similarity to that of tetrahedral, framework Ga in MFI-type gallosilicate.[27] In the extended X-ray absorption fine structure (EXAFS), the feature at 1.6 Å in *R*-space (not phase-corrected) is caused by scattering by light atoms (C, O) directly bonded to Ga (Figure 2a). The feature at 2.6 Å resembles the peak seen in the EXAFS of $[(CH_3)_2Ga(\mu\text{-}OSi(C_6H_5)_3)]_2$, where it arises from a Ga−Ga single-scattering path across the planar Ga_2O_2 ring.[20] Thus, despite the apparent isolation of the hydroxyl groups on A380-800, as judged by the absence of discernible hydrogen-bonding between them in the IR spectrum, their reaction with $Ga(CH_3)_3$ appears to yield a significant number of paired grafted sites.

A curve fit of the EXAFS was obtained using a free energy force field (FEFF) model generated from the single-crystal X-ray structure of $[Ga(CH_3)_2(\mu\text{-}OSi(C_6H_5)_3)]_2$.[20] The results are shown in Figure 2 and Table 1. Since the Ga−C and Ga−O distances are too similar to be resolved, a single Ga−C path (N = 4) was used to represent both Ga−C and Ga−O paths. The refined average Ga−C/O distance, 1.95 Å, is consistent with terminal, rather than bridging, methyl groups. In heterobimetallic complexes containing the fragment $(CH_3)_2Ga(\mu\text{-}CH_3)M$ (where M = Zr, Nd, La), the bridging Ga−C bonds (2.033−2.142 Å) are considerably longer than the terminal Ga−C bonds (1.968−1.984 Å).[28,29] Furthermore, the fitted Ga−C/O distance is comparable to the Ga−O distances in molecular

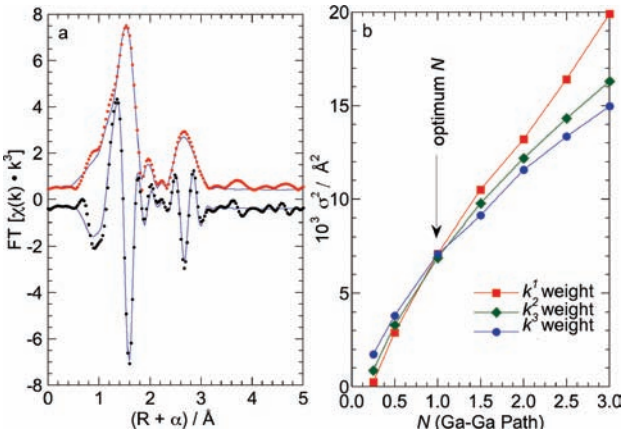

Figure 2. (a) Ga K-edge EXAFS (FT magnitude, red; imaginary, black) for $Ga(CH_3)_3$-modified silica (A380-800), showing the curve fit to a model based on $[Ga(CH_3)_2(\mu\text{-}OSi(C_6H_5)_3)]_2$ (blue), with fixed N = 1 for the Ga−Ga path. (b) Analysis of the optimum value of N for the Ga−Ga path via the correlation-break method.[31]

compounds containing the $Ga_2(\mu\text{-}O)_2$ "diamond" core, for which d(Ga−O) is reported to range from 1.91 to 1.97 Å.[20,30] In contrast, terminal Ga−O bonds in the same compounds are considerably shorter, 1.81−1.85 Å. The EXAFS is therefore consistent with grafted digallium sites bridged by silanolate ligands.

All of the interatomic distances, including the Ga−Ga distance of 2.99 Å, are very similar to those of the molecular dimer (SI, Table S1), suggesting that the silica-supported sites are also organized into Ga_2O_2 rings. Unlike $Al(CH_3)_3$, which exists as a dimer in both the gas and condensed phases at room temperature,[33] $Ga(CH_3)_3$ is monomeric in both phases.[34,35] The dimeric nature of the silanolate-bridged digallium sites must therefore be imposed by the silica surface.

When the prominent EXAFS feature at 2.6 Å in the FT magnitude was refined to other possible single-scattering (i.e., Ga−O, Ga−Si) or multiple-scattering paths (i.e., Ga−C−C), all gave unacceptably large Debye−Waller factors and failed to reproduce the *R*-space intensity (SI, Figures S5 and S6). However, since curve-fitting analysis of the EXAFS is necessarily model-dependent, further confirmation of the identity of the Ga−Ga scattering path was sought using the wavelet transform (WT).[36] When the Fourier transform (FT) is applied to an EXAFS data set, no correlations exist between the resulting *R*-space data and the original *k*-space data because the sine waves used in the FT operation are continuous and infinite. The WT uses instead a discrete wavelet with a comparatively small *k*-range, allowing correlations to be made between *R*- and *k*-space forms of the data.[37] This wavelet is sequentially stretched and scaled through the data set to locate maxima in the convolution function of the *k*-space data with the wavelet. The locations of maxima in the WT modulus are very sensitive to atomic number, which (in simple cases) facilitates identification of the maxima with the scattering atoms that generate them. Recently, a Ga−Ga path was distinguished from Ga−Fe paths in the EXAFS of Ga(III) adsorbed on goethite by Continuous Cauchy Wavelet Transform (CCWT) analysis.[38] The Morlet Wavelet Transform (MWT) has also been used in the qualitative analysis of EXAFS spectra[39] and has the advantage of allowing resolution to be optimized in *k*-space as well as in *R*-space.

Figure 3 shows the MWT modulus for the EXAFS of $Ga(CH_3)_3$-modified A380-800 silica. The feature at ca. 1.5 Å in

dx.doi.org/10.1021/ja108905p | *J. Am. Chem. Soc.* 2011, 133, 4847–4855

Table 1. Comparison of EXAFS Curve Fit Parameters for $Ga(CH_3)_3$-Modified A380-800 Silicas, with Interatomic Distances from Computational Model Structures

		EXAFS curve fit			DFT model	
sample	path	N^a	R/Å	$10^3\,\sigma^2$/Å^2	N	d/Å
grafted $Ga(CH_3)_3$[b]	Ga−C	4[c]	1.95 ± 0.06	5 ± 1	2	1.96[d]
	Ga−O				2	2.01[d]
	Ga−Ga	1	2.99 ± 0.05	6 ± 1	1	2.89[d]
after exposure to NH_3[e]	Ga−O	3[f]	1.95 ± 0.06	5 ± 1	1	1.91[g]
	Ga−C				2	1.98[g]
	Ga−N	1	2.06 ± 0.07	9 ± 3	1	2.07[g]

[a] Integer values of N were not refined. [b] Global fit parameters: $S_0^2 = 0.83 \pm 0.03$; $\Delta E_0 = 0.81 \pm 0.2$ eV; residuals = 11. Number of independent parameters used in the fit: 6 (of 26 allowed by the Nyquist theorem).[32] [c] Ga−O and Ga−C paths were combined and modeled as one Ga−C path ($N = 4$). [d] Distances are from the energy-minimized structure of DFT model **3** (see Figure 5). [e] Global fit parameters: $S_0^2 = 0.87 \pm 0.13$; $\Delta E_0 = 0.38 \pm 0.21$ eV; residuals = 76. Number of independent parameters used in the fit: 8 (of 26 allowed by the Nyquist theorem).[32] [f] Ga−O and Ga−C paths were combined and modeled as one Ga−O path ($N = 3$). [g] Distances are from the energy-minimized structure of DFT model **4** (see Figure 5).

R-space gives a maximum in the MWT modulus at 5.3 Å^{-1} in *k*-space, consistent with scattering by low-*Z* atoms (C, O). The feature at ca. 2.7 Å in *R*-space corresponds to a maximum in the backscattering amplitude at 8.0 Å^{-1} in *k*-space. The simulated WT of a Ga−Ga scattering path at 3.0 Å produces a maximum at 7.9 Å^{-1} in *k*-space, compared to 6.3 and 5.5 Å^{-1} for Ga−Si and Ga−O paths, respectively (SI, Figures S15−S17). The nonbonded scatterer responsible for the intensity in the FT magnitude at 2.6 Å is thereby positively identified as Ga.

The fraction of grafted dimethylgallium(III) sites that is dimeric is equal to the coordination number N for the Ga−Ga scattering path. In the EXAFS curve fit, N is strongly correlated with the mean-squared displacement σ^2. Their optimum values were investigated by correlation break analysis: when σ^2 is refined using various *k*-weights, the values converge at the best value for N.[31] According to Figure 2b, this occurs at $N = 1.0$; i.e., essentially all of the grafted dimethylgallium sites on A380-800 silica are dimeric. This result further implies that all of the grafting sites on the silica surface are present in pairs, instead of being isolated or randomly distributed.

Nature of the Paired Grafting Sites. The high probability of Ga dimer formation on highly dehydroxylated silicas cannot be explained by migration of the surface hydroxyl groups, which are not mobile.[12,14,15] Nor is it likely that the $Ga(CH_3)_2$ fragments migrate at room temperature, since this would require cleavage of strong Ga−O and Si−O bonds. Instead, protonolysis of $Ga(CH_3)_3$ by an isolated silanol must be accompanied by the reaction of a second $Ga(CH_3)_3$ molecule with an adjacent siloxane bond, resulting in methyl group transfer to silicon, eq 2.

$$\equiv SiOH + \equiv SiOSi\equiv + 2Ga(CH_3)_3 \rightarrow [(CH_3)_2Ga(\mu\text{-}OSi\equiv)]_2 + CH_3Si\equiv + CH_4 \qquad (2)$$

The high uniformity of the Ga_2O_2 rings that is evident in the fit parameters for the Ga−Ga path ($N = 1.0$; $\sigma^2 = 0.006 \pm 0.001$ Å^2) suggests a precise relationship between the silanol and the reactive siloxane bond. During silica pretreatment at 800 °C, condensation of a vicinal pair of silanols (i.e., those separated by a single bridging oxygen) leads to the formation of a highly strained 2-ring (Si_2O_2).[18,40] When one of the silanols is also a member of a geminal silanol pair (i.e., a vicinal Q^2−Q^3 site pair), the result is a 2-ring with a hydroxyl substituent, as shown in eq 3.

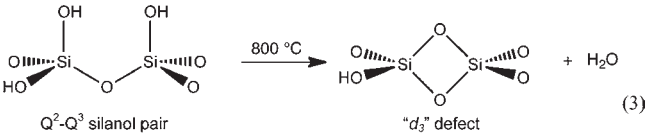

(3)

Geminal silanols (Q^2 sites) have been observed by ^{29}Si cross-polarization magic angle spinning (CP-MAS) NMR on fumed silicas dehydroxylated at temperatures up to 800 °C.[41] Porous silica gels such as the Sylopols are also known to have significant geminal silanol populations.[42] As the silicas are heated, 2-rings first arise via the condensation reaction shown in eq 3, since they impose less strain on the silica framework than do 2-rings lacking a hydroxyl substituent (i.e., which are anchored via an additional siloxane linkage to the lattice).[40] The proposed reaction of $Ga(CH_3)_3$ with a hydroxyl-substituted 2-ring is depicted in eq 4.

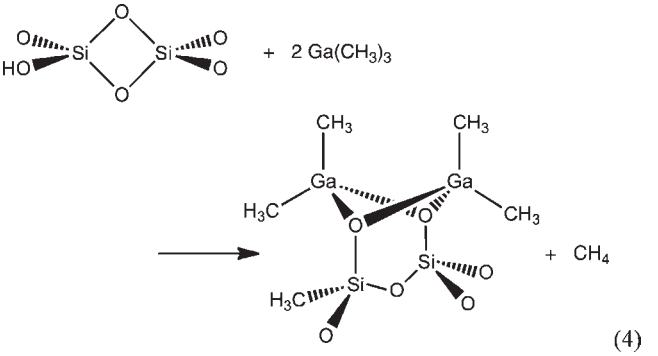

(4)

It is possible that siloxane bond cleavage occurs prior to protonolysis of $Ga(CH_3)_3$ by the remaining silanol, due to the very high reactivity of the strained 2-rings.[40]

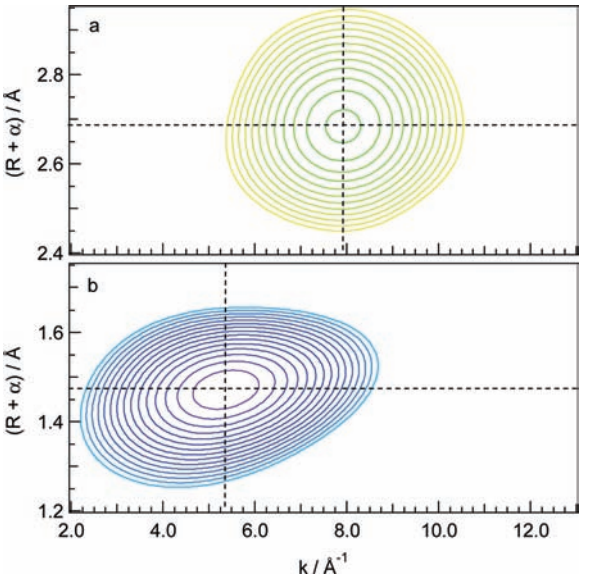

Figure 3. Morlet Wavelet Transform (MWT) analysis ($\kappa = 10, \sigma = 1$) of the Ga K-edge EXAFS for $Ga(CH_3)_3$-modified A380-800, showing the maxima in the MWT modulus in the regions of (a) the Ga−Ga path and (b) the Ga−O/Ga−C paths.

dx.doi.org/10.1021/ja108905p | *J. Am. Chem. Soc.* 2011, 133, 4847–4855

Evidence for Silicon Methylation. The ^{1}H MAS NMR spectrum of $Ga(CH_3)_3$-modified A380-800 shows only a broad signal at −1.0 ppm (Figure 4a). However, signals for both $GaCH_3$ (8.7 ppm) and O_3SiCH_3 (−12.3 ppm) are resolved in the ^{13}C CP-MAS NMR spectrum (Figure 4b). The $SiCH_3$ signals are even clearer after exhaustive hydrolysis (heating at 200 °C for 2 h in the presence of excess water vapor, followed by evacuation at the same temperature for 2 h). The expected hydrolysis reaction, which cleaves Ga−CH_3 bonds but leaves Si−CH_3 bonds intact, is shown in eq 5.

$$[(CH_3)_2Ga(\mu\text{-}OSi\equiv)]_2 + CH_3Si\equiv + 4H_2O \rightarrow 2\text{“}(\equiv SiO)Ga(OH)_2\text{”} + CH_3Si\equiv + 4CH_4 \quad (5)$$

The ^{1}H MAS NMR spectrum of the hydrolyzed material presents two major signals: −1.1 ppm ($\equiv SiCH_3$)[43] and 0.7 ppm (assigned to $GaOH$)[44] (Figure 4c). In the post-hydrolysis ^{13}C CP-MAS NMR spectrum (Figure 4d), the signal assigned to $GaCH_3$ is no longer present, while the signal of the non-hydrolyzable O_3SiCH_3 sites remains. The presumed “$(\equiv SiO)Ga(OH)_2$” product, which likely oligomerizes, was not characterized further.

Since CP-MAS NMR spectra are not inherently quantitative, the extent of silicon methylation by $Ga(CH_3)_3$ was investigated via the mass balance. The $Ga(CH_3)_3$-modified A380-800 contains 0.64 ± 0.07 mmol of Ga/g of SiO_2, which is 50% higher than the hydroxyl content of the unmodified silica. By comparison to the observed methane yield, 0.43 mmol/g of SiO_2, we infer that two-thirds of the grafted $Ga(CH_3)_3$ reacted directly with a surface hydroxyl, while one-third was anchored via reaction with a siloxane bond. Upon hydrolysis, 1.13 ± 0.09 of mmol of CH_4/g of silica was liberated, for a CH_4/Ga ratio of 1.76 ± 0.26. Thus, essentially all the grafted gallium sites bear two methyl ligands, regardless of whether they were originally anchored by reaction with a silanol or a siloxane.

The mass balance shows that half of the Ga dimers on A380-800 silica arise by combined siloxane cleavage/protonolysis (as in eq 2). The rest are formed solely by protonolysis, requiring two silanol sites (as in eq 1). The persistence of silanol pairs, despite their very low surface density and the absence of any detectable interactions between them in the IR spectrum, is consistent with their identification as vicinal Q^3−Q^3 pairs. These do not form mutual hydrogen bonds, and, unlike the vicinal Q^2−Q^3 sites, they do not undergo mutual condensation at or below 800 °C,[40] eq 6.

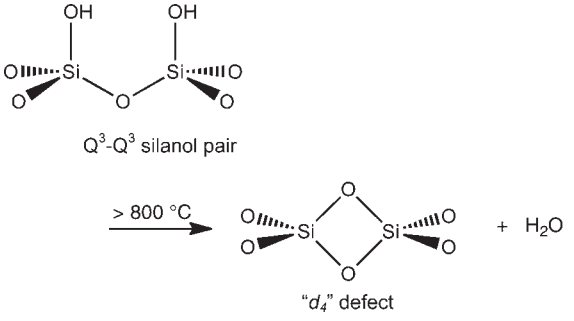

(6)

The reaction of $Ga(CH_3)_3$ with a vicinal Q^3−Q^3 pair gives rise to the site $[(CH_3)_2Ga]_2(\mu\text{-}OSi\equiv)_2O$, in which the silicon atoms are directly connected by a bridging oxygen. It differs from the dimer formed by reaction of 2 equiv of $Ga(CH_3)_3$ with a hydroxyl-substituted 2-ring only by the absence of the methyl group attached to silicon. The two dimer sites are therefore expected to be indistinguishable by Ga K-edge EXAFS.

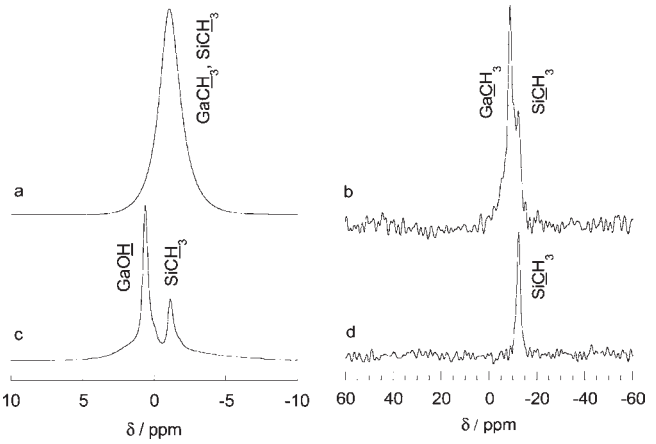

Figure 4. Solid-state ^{1}H MAS (left) and ^{13}C CP-MAS (right) NMR spectra of $Ga(CH_3)_3$-modified A380-800 silica, before (a,b) and after (c,d) hydrolysis at 200 °C, with evacuation of volatiles at the same temperature.

Reaction of A380-800 Silica with a Limiting Amount of $Ga(CH_3)_3$. The reaction of A380-800 with $Ga(CH_3)_3$ is self-limiting, ceasing when all accessible grafting sites on the silica surface have been consumed. When A380-800 is exposed to excess $Ga(CH_3)_3$ vapor, the maximum uptake corresponds to 4.2 wt % Ga, representing complete reaction of the organometallic complex with the grafting sites. We also investigated the reaction with a limiting amount of $Ga(CH_3)_3$, in order to probe whether isolated or paired dimethylgallium sites are formed at low surface coverage. For a material containing only 1.1 wt % Ga, the EXAFS and fit parameters are shown in the SI, Figures S11 and S12 and Table S5. They show the prominent Ga−Ga scattering path at 2.6 Å in *R*-space. Correlation break analysis gave an optimum value for *N* of 1.05 for this path (SI, Figure S13). We conclude that the formation of silanolate-bridged dimers occurs even when unreacted grafting sites are still available.

The preferred formation of grafted Ga dimers at low surface coverage implies that attachment of the first $Ga(CH_3)_2$ fragment to silica, via either cleavage of a strained siloxane bond or reaction with a surface silanol, activates the vicinal silanol. Coordination of this silanol to the adjacent $Ga(CH_3)_2$ site, eq 7, would increase its acidity, making it more reactive toward a second equivalent of $Ga(CH_3)_3$.

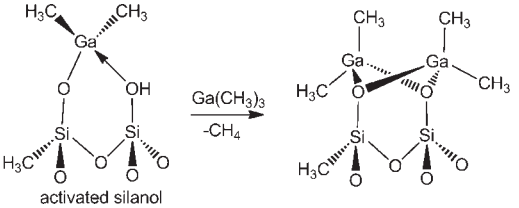

(7)

Computational Model Structures. The feasibility of forming disilanolate-bridged bis(dimethylgallium) sites was explored computationally. Figure 5 shows the H-terminated silanol clusters used to model the condensation product of a Q^2−Q^3 site (**1**), as well as a Q^3−Q^3 site pair (**5**). Reaction with $Ga(CH_3)_3$ with **1**, resulting in cleavage of the strained siloxane ring by

dx.doi.org/10.1021/ja108905p |*J. Am. Chem. Soc.* 2011, 133, 4847–4855

$Ga(CH_3)_3$ with methyl transfer to Si and replacement of the silanol proton by $Ga(CH_3)_2$ with release of CH_4, is energetically favorable (ΔE = −420 kJ/mol), even without formation of the silanolate bridges. The terminal Ga−O distance in **2** is 1.80 Å. The tricoordinate Ga atoms exhibit long Ga···CH_3 interactions (3.03 Å).[45]

Rearrangement of model **2** to model **3**, which has symmetrical silanolate bridges at d(Ga−O) = 2.01 Å, is favored by 100 kJ/mol. The Ga_2O_2 ring has a dihedral angle of 33° and a Ga−Ga distance of 2.89 Å. Formation of the silanolate bridges in **3** causes the SiOSi angle to decrease to 130°, while the distance between the silanolate oxygens contracts to 2.56 Å. The OSiO angles, at 104°, are slightly smaller than tetrahedral, indicating ring strain. While changes in OSiO angles are typically minor, SiOSi angles in silicate minerals and silica polymorphs vary from 137 to 175°,[46] and their deformation involves only minor changes in energy.[47] The reaction of $Ga(CH_3)_3$ with the vicinal disilanol **5** results in the dimer **6**, whose structural parameters are very similar to those of **3**. The formation of both Ga dimers is a direct consequence of the strong Lewis acidity of three-coordinate Ga, which leads to the formation of silanolate bridges and creates the Ga_2O_2 ring whose Ga−Ga scattering path is readily detected by EXAFS.

Latent Lewis Acidity. Silicas modified with $M(CH_3)_3$ (M = Al, Ga) are strongly Lewis acidic; their acidity has been attributed to the presence of three-coordinate metal sites.[22,48,49] The X-ray absorption near-edge structure (XANES) and EXAFS indicate that the grafted Ga sites are four-coordinate. Nevertheless, they are reactive toward Lewis bases. Upon exposure of $Ga(CH_3)_3$-modified A380-800 to NH_3(g) at room temperature (NH_3/Ga ≈ 10), no methane was detected by *in situ* IR. Bands characteristic of the N−H stretching modes of adsorbed NH_3 appeared at 3375 and 3290 cm^{-1} in the IR spectrum (not shown), and a dramatic change in the intensity of the *R*-space feature at 2.6 Å was observed in the Ga K-edge EXAFS (Figure 6). This is consistent with disruption of the bridging silanolate interactions upon coordination of the Lewis base, resulting in loss of coherence for the Ga−Ga scattering path. Heating the sample to 200 °C under dynamic vacuum resulted in little change in either the IR or EXAFS spectra, demonstrating that the coordination of NH_3 is irreversible for this material.

In agreement with our observation that NH_3 binds strongly to $Ga(CH_3)_3$-modified silica, coordination of NH_3 to **3** to give the adduct **4** was computed to be energetically favorable (ΔE = −161 kJ/mol, Figure 5). The Ga−O bonds contract from 2.01 to 1.91 Å when the silanolate bridges are disrupted by NH_3. The resulting Ga−N bond lengths are 2.07 Å. The Ga−Ga distance is elongated to 4.59 Å, while the SiOSi angle increases slightly to 137°. This calculated structure is consistent with the EXAFS of $Ga(CH_3)_3$-modified silica after its exposure to NH_3. The curve fit using a FEFF model based on **4** is shown in Figure 7, and fit parameters are given in Table 1. The refined Ga−N distance, 2.06 Å, agrees with the Ga−N bond length in the calculated structure but is considerably shorter than the Ga−N distance in $(CH_3)_3Ga{\cdot}NH_3$ (2.16 Å).[50]

The disilanolate-bridged Ga dimers therefore possess significant, albeit latent,[51] Lewis acidity. The disappearance of the Ga−Ga path in the EXAFS upon NH_3 exposure is consistent with the presence of pairs of Ga sites that are no longer Lewis acidic and that lack coherent Ga−Ga scattering paths. In general, grafted metal complexes that are not strongly Lewis acidic or whose ligand complement precludes bridging interactions may appear to be well-separated by EXAFS even when they are paired; the failure to observe M−M scattering is insufficient evidence for site isolation.

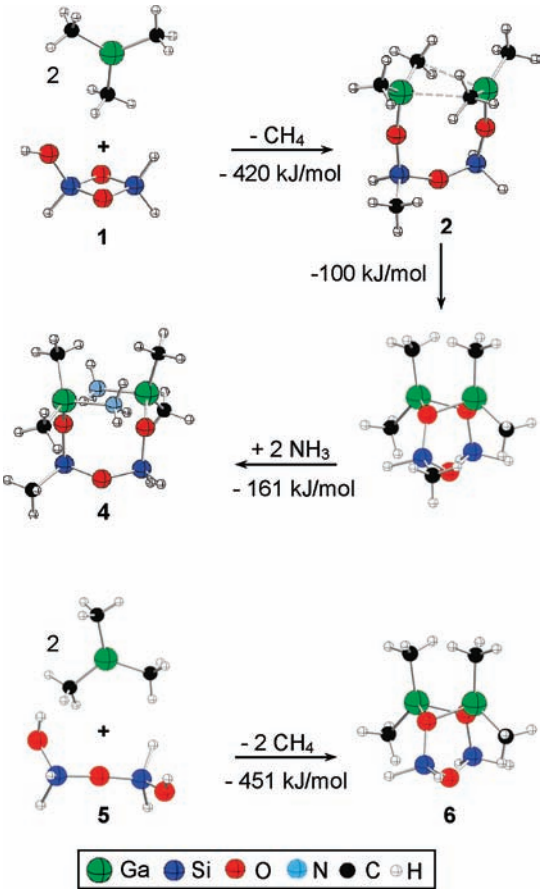

Figure 5. Cluster models and DFT-computed energies (ΔE) for the reactions of $Ga(CH_3)_3$ with a hydroxyl-substituted siloxane 2-ring (**1**) and a vicinal disilanol (**5**), leading to the disilanolate-bridged structures **3** and **6**, respectively, as well as disruption of the bridging silanolate interactions in **3** by coordination of NH_3 (**4**).

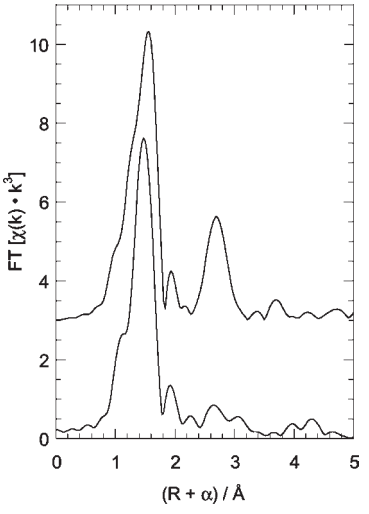

Figure 6. Comparison of Ga K-edge EXAFS (FT magnitude) for $Ga(CH_3)_3$-modified A380-800, before (top) and after (bottom) exposure to 10 equiv of NH_3.

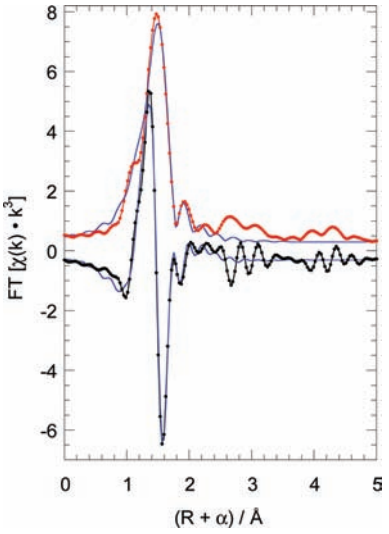

Figure 7. Ga K-edge EXAFS (FT magnitude, red; imaginary, black) for $Ga(CH_3)_3$-modified A380-800 after exposure to 10 equiv of NH_3 and curve fit (blue), generated using model **4**.

Reaction of $Ga(CH_3)_3$ with Porous Silica. The formation of Ga dimers is not unique to fumed silica. The Ga K-edge EXAFS reveals the existence of similar structures when $Ga(CH_3)_3$ was used to modify a mesoporous silica gel (Sylopol 952), after its pretreatment *in vacuo* at 800 °C. The white-line intensity in the XANES for this material strongly resembles that of $Ga(CH_3)_3$-modified A380-800, and is also consistent with four-coordinate Ga (SI, Figure S7).[27] The *R*-space EXAFS contains a strong Ga−Ga path (SI, Figure S9), and the MWT of the EXAFS is consistent with the presence of a Ga−Ga path (SI, Figure S18). Although the optimum fitted value of *N* for the Ga−Ga path is less than 1.0 (SI, Table S4), a significant fraction (about half) of the grafted sites on the highly dehydroxylated silica gel are disilanolate-bridged dimers. The high surface curvature[52,53] of the Sylopol, compared to the relatively flat surface of the fumed silica, may allow some $Ga(CH_3)_2$ pairs to achieve tetra-coordination by interacting with surface siloxane oxygens instead. This precludes a fixed Ga−Ga distance but does not imply that the sites are isolated.

CONCLUSIONS

Dehydroxylation of both porous and nonporous silica at 800 °C yields surface hydroxyl groups that, while isolated, are nevertheless closely associated with reactive siloxane bonds, probably as hydroxyl-substituted 2-rings formed by condensation within vicinal Q^2−Q^3 pairs. Their reaction with $Ga(CH_3)_3$ leads to $[(CH_3)_2Ga]_2(\mu\text{-OSi}\equiv)(\mu\text{-OSi}(CH_3)=)$, rather than isolated dimethylgallium fragments. This reaction accounts for about half of the grafted Ga sites formed on A380-800. The other half is formed by reactions with vicinal hydroxyl groups, which are Q^3−Q^3 pairs whose condensation to form 2-rings does not occur at 800 °C. Thus, two-thirds of the hydroxyl groups on this highly dehydroxylated silica are not isolated, being located close to (although not hydrogen-bonded to) a neighboring silanol group. During the high-temperature synthesis of fumed silica, hydrolysis of highly strained siloxane bonds gives rise to such silanol pairs.[54] On the mesoporous Sylopol silica, a significant fraction of the grafted Ga sites are also dimers, implying extensive pairing of the surface hydroxyls, even after pretreatment at 800 °C.

Consequently, the residual silanol groups on these highly dehydroxylated, amorphous silicas should not be described as randomly distributed or well-separated: the median interhydroxyl distance, at ca. 3 Å, is considerably smaller than the mean (12 Å). Site isolation by simple thermal dehydroxylation of these silicas does not appear to be feasible: even "isolated" hydroxyl groups are located in close proximity to a second grafting site (the strained, highly reactive siloxane bond of a 2-ring). Pairwise grafting is therefore inevitable, even when the absence of coherent metal−metal single-scattering paths precludes its direct observation by EXAFS. These findings have broad implications for site isolation strategies as well as for cooperative grafting of functional groups by surface modification in catalysis and other silica applications.

EXPERIMENTAL AND COMPUTATIONAL METHODS

Sample Preparation. Aerosil 380, a nonporous, fumed silica, was obtained from Evonik-Degussa. It has a BET surface area of 383 ± 14 m^2/g and an average primary particle size of 7 nm. It was pretreated by calcining in air at 500 °C for at least 3 h, followed by partial dehydroxylation at 800 °C for at least 4 h under dynamic vacuum ($<10^{-4}$ Torr) to give A380-800. Sylopol 952, a nonordered mesoporous silica gel, was obtained from Grace-Davison. It has a BET surface area of 300 ± 18 m^2/g, a pore volume of 1.61 mL/g, and an average particle size of 112 μm. It was pretreated by calcination at 450 °C in flowing O_2 for 4 h, followed by evacuation at the same temperature for 2 h. The silica was subsequently dehydroxylated at 800 °C for at least 4 h under dynamic vacuum to give S952-800.

$Ga(CH_3)_3$ (Strem, 99.9%) was stored under vacuum in a glass reactor sealed with two high-vacuum Teflon stopcocks (Chemglass) arranged in series. ***Caution!*** *$Ga(CH_3)_3$ is pyrophoric and should only be handled in small quantities (<1 mL) outside a glovebox.* Milli-Q water was transferred into a high-vacuum glass reactor sealed with a ground-glass stopcock greased with Krytox (Varian). Both $Ga(CH_3)_3$ and H_2O were subjected to three freeze−pump−thaw cycles before each use. NH_3(g) (Praxair, 99.99%) was transferred via a high-vacuum manifold into a glass bulb containing activated molecular sieves to remove moisture and sealed with a high-vacuum ground-glass stopcock greased with Apiezon-H (Varian).

Reagents were transferred onto the silicas through a high-vacuum manifold, using a quartz reactor immersed in a liquid N_2 bath. After warming to room temperature, excess $Ga(CH_3)_3$ was allowed to react with silica for 20 min. Volatiles were desorbed at room temperature to a liquid N_2 trap for 30 min. When NH_3(g) was transferred onto the $Ga(CH_3)_3$-modifed silica, the reaction was allowed to proceed at room temperature for 2 h. When the reactor was subsequently evacuated at room temperature for 6 h.

Infrared Spectroscopy. IR experiments were performed in a Pyrex *in situ* IR cell equipped with a quartz bottom and sealed with a high-vacuum ground-glass stopcock greased with Krytox (Varian). Polished CaF_2 windows (32 × 2 mm, International Crystal Laboratories) were affixed to the cell with TorrSeal (Varian). Approximately 25 mg of A380 silica was pressed in air into a self-supporting disk of diameter 1.6 cm and then mounted in a quartz sample holder. The silica was heated in air at 500 °C for at least 4 h prior to dehydroxylation at $>10^{-4}$ Torr and at 800 °C for at least 4 h. $Ga(CH_3)_3$ vapor was transferred onto the silica from a liquid reservoir, using a liquid nitrogen bath. The reactor was allowed to warm to room temperature over a period of 20 min. Transmission IR spectra were recorded on a Shimadzu Prestige IR spectrometer equipped with a DTGS detector and purged with CO_2-free dry air. Background and sample spectra were recorded by adding 24 scans at 2 cm^{-1} resolution (for spectra of silicas) and 0.5 cm^{-1} resolution (for spectra of CH_4(g)).

dx.doi.org/10.1021/ja108905p |*J. Am. Chem. Soc.* 2011, 133, 4847–4855

Mass Balance. The amount of methane liberated during grafting and subsequent hydrolysis of $Ga(CH_3)_3$ was determined by *in situ* IR spectroscopy. A calibration curve in the range 0.2−20 Torr was constructed using the absorbance of the CH_4 stretching mode at 3016 cm^{-1}. After each experiment, the silica sample was weighed in air and stirred overnight in 1.0 M H_2SO_4. The suspension was centrifuged to remove the silica, and the Ga content of the supernatant was determined by ICP (Thermo iCAP 6300). A calibration curve was constructed in the range 0−40 ppm by diluting a standard solution (Fluka, 1000 ppm Ga).

X-ray Absorption Spectroscopy. Spectra were recorded at the Ga K-edge (10.367 keV) on beamline 2-3 (Bend) at the Stanford Synchrotron Radiation Lightsource (SSRL), which operates at 3.0 GeV with a ring current of 80−100 mA. X-rays were monochromatized via reflection from a pair of Si(220) crystals through a 2 mm entrance slit. The incident beam was detuned by 30% to remove harmonics. Samples were mounted at a 45° angle to the beam in order to collect transmission and fluorescence spectra simultaneously. Spectra were recorded at 10 K in an Oxford Instruments liquid He flow cryostat. Fluorescence data were generally of better spectral quality than transmission data and were therefore used in data analysis.

Data processing and analysis were performed using Athena (version 0.8.056) and Artemis (version 0.8.012).[55] Single-scattering paths were fitted to the *R*-space data using least-squares refinement. Phase shift and backscattering amplitude functions were calculated using FEFF 8.2.[56] Morlet Wavelet Transform calculations were performed using the Python (version 2.6) program HAMA written for the wavelet transform analysis and simulation of EXAFS data.[37]

Solid-State NMR Spectroscopy. Solid-state ^1H and ^{13}C NMR spectra were recorded on a Bruker ASX-500 spectrometer. First, 100−200 mg of silica was compressed into thick pellets that were then ground coarsely using a mortar-and-pestle. After reaction with $Ga(CH_3)_3$, samples were loaded into 4 mm zirconia rotors under Ar. ^1H MAS NMR spectra were recorded at 500.12 MHz. The spectra were collected using a 2-μs 4° pulse, a relaxation delay of 0.15 s, and an acquisition time of 25 ms. ^{13}C CP-MAS NMR spectra were recorded at 125.47 MHz using a contact time of 2 ms and a relaxation delay of 2 s. All rotors were spun at 10 kHz. ^{13}C-labeled glycine (Cambridge Isotope Laboratories, Inc.) was used as the external chemical shift reference for both ^1H and ^{13}C. Spectra were baseline corrected, and 3 Hz line broadening was applied to the ^{13}C spectra.

Measurement of the Hydroxyl Content of Dehydroxylated Silicas. To avoid any transfer of material that would expose highly strained, reactive siloxane bonds to traces of moisture (e.g., in a glovebox), the number of hydroxyls present in A380-800 silica was determined from the area of the O−H stretching mode in the *in situ* IR spectrum (Figure 1) relative to the area in a sample of known OH content.

First, the number of non-hydrogen-bonded hydroxyl groups in A380-500 silica was measured. The solid-state ^1H MAS NMR spectrum of a known mass of the silica was recorded under Ar, and the total OH content was obtained by comparison to the ^1H MAS NMR spectrum of an external standard, tetrakis(trimethylsilyl)silane. This experiment was repeated after complete reaction of the accessible hydroxyls of A380-500 with $VOCl_3$ (99.995%, Aldrich),[57] yielding the number of inaccessible hydroxyls. The number of accessible hydroxyl groups was obtained by difference.

The area of the O−H stretching region in the IR spectrum of A380-500 was measured before and after reaction with $VOCl_3$. The number of hydroxyls present in A380-800 was calculated from the ratio of the areas for A380-500 and A380-800, using the intensity of the lattice overtone at 1875 cm^{-1} to normalize the spectra for the amount of silica present. The hydroxyl content for S952-800 was determined by comparing the area under the O−H stretching region of a normalized S952-800 spectrum to that of the normalized A380-800 spectrum. This gives the hydroxyl number normalized to the amount of silica in the sample. This hydroxyl number was corrected for the difference in surface areas between the two silicas to obtain the hydroxyl number per surface area on S952-800.

Computational Methods. Geometry optimizations and energy calculations for model compounds were performed with Gaussian03,[58] using the hybrid exchange functional B3LYP.[59,60] The Gaussian basis set 6-31+G* was used for all elements. Stationary points were characterized by the calculation of vibrational frequencies, and all geometries were found to be minimum energy structures ($N_{imaginary} = 0$).

■ ASSOCIATED CONTENT

Supporting Information. Experimental and computational methods, additional EXAFS curve fits, fit parameters, wavelet transforms, Cartesian coordinates of calculated structures, and complete refs 10 and 58. This material is available free of charge via the Internet at http://pubs.acs.org.

■ AUTHOR INFORMATION

Corresponding Author
sscott@engineering.ucsb.edu

■ ACKNOWLEDGMENT

We are grateful to Prof. Harald Funke and Dr. Marina Chukalina for the Python script used in the Morlet Wavelet Transform analysis, and to Dr. Ming-Yung Lee for the quantitative analysis of silica hydroxyl content. This work was funded by the Catalysis Science Initiative of the U.S. Department of Energy, Basic Energy Sciences (award No. DE-FG02-03ER15467). S.F. is grateful for a fellowship from the PIRE-ECCI program, supported by the National Science Foundation under award no. OISE-0530268. Portions of this work were performed at the Stanford Synchrotron Radiation Lightsource, a national user facility operated by Stanford University on behalf of the U.S. Department of Energy, Office of Basic Energy Sciences, and at the MRL Central Facilities, supported by the MRSEC Program of the National Science Foundation under award no. DMR05-20415.

■ REFERENCES

(1) Green, M. L.; Gusev, E. P.; Degraeve, R.; Garfunkel, E. L. *J. Appl. Phys.* **2001**, *90*, 2057–2121.
(2) Hess, D. W. *Electrochem. Soc. Interface* **2009**, *18*, 48–50.
(3) Unger, K. K. *Porous Silica—Its Properties and Use as a Support in Column Liquid Chromatography*; Elsevier: Amsterdam, 1979; Vol. 16.
(4) Ernst-Cabrera, K.; Wilchek, M. *Anal. Biochem.* **1986**, *159*, 267–272.
(5) Tomozawa, M.; Hepburn, R. W. *J. Non-Cryst. Solids* **2004**, *345−346*, 449–460.
(6) Zou, H.; Wu, S.; Shen, J. *Chem. Rev.* **2008**, *108*, 3893–3957.
(7) Caro, J.; Doudkowsky, M.; Figueras, A.; Fraxedas, J.; Garcia, G.; Santiso, J.; Schamm, S.; Ojeda, F.; Vazquez, L.; Albella, J. M. In *Handbook of Surfaces and Interfaces of Materials*; Nalwa, H. S., Ed.; Academic Press: San Diego, CA, 2001; Vol. 4, pp 229−280.
(8) Scott, S. L.; Basset, J.-M.; Niccolai, G. P.; Santini, C. C.; Candy, J.-P. Lecuyer, C.; Quignard, F.; Choplin, A. *New J. Chem.* **1994**, *18* 115–122.
(9) Scott, S. L., Crudden, C. M., Jones, C. W., Eds.; *Nanostructured Catalysts*; Kluwer: New York, 2003.
(10) Bassett, J.-M. et al. In *Modern Surface Organometallic Chemistry*; Basset, J.-M., Psaro, R., Roberto, D. Ugo, R., Eds.; Wiley-VCH: Weinheim, 2009; pp 23−73.
(11) Hartley, F. R. *Supported Metal Complexes*; D. Reidel: Holland, 1985.
(12) Iler, R. K. *The Chemistry of Silica: Solubility, Polymerization, Colloid and Surface Properties and Biochemistry of Silica*; Wiley: New York, 1979.

(13) Peri, J. B. *J. Phys. Chem.* **1966**, *70*, 2937–2945.
(14) Doremus, R. H. *J. Mater. Res.* **1995**, *10*, 2379–2389.
(15) Van Ginhoven, R. M.; Jonsson, H.; Park, B.; Corrales, L. R. *J. Phys. Chem. B* **2005**, *109*, 10936–10945.
(16) Morrow, B. A. In *Studies in Surface Science and Catalysis*; Fierro, J. L. G., Ed.; Elsevier: Amsterdam, 1990; Vol. 57A, pp 161−224.
(17) Zhuravlev, L. T. *Langmuir* **1987**, *3*, 316–318.
(18) Morrow, B. A.; Cody, I. A. *J. Phys. Chem.* **1976**, *80*, 1995–1998.
(19) Morrow, B. A.; McFarlan, A. J. *J. Phys. Chem.* **1992**, *96* 1395–1400.
(20) Taha, Z. A.; Deguns, E. W.; Chattopadhyay, S.; Scott, S. L. *Organometallics* **2006**, *25*, 1891–1899.
(21) Schmidbaur, H.; Schindler, F. *Chem. Ber* **1966**, *99*, 2178–2186.
(22) Hlatky, G. G. *Chem. Rev.* **2000**, *100*, 1347–1376.
(23) Serp, P.; Kalck, P.; Feurer, R. *Chem. Rev.* **2002**, *102*, 3085–3128.
(24) Dubois, L. H.; Zegarski, B. R. *J. Am. Chem. Soc.* **1993**, *115*, 1190–1191.
(25) Grabbe, A.; Michalske, T. A.; Smith, W. L. *J. Phys. Chem.* **1995**, *99*, 4648–4654.
(26) Gladden, L. F.; Vignaux, M.; Chiaranussati, P.; Griffiths, R. W.; Jackson, S. D.; Jones, J. R.; Sharratt, A. P.; Robertson, F. J.; Webb, G.; Chieux, P.; Hannon, A. C. *J. Non-Cryst. Solids* **1992**, *139*, 47–59.
(27) Nishi, K.; Shimizu, K.-I.; Takamatsu, M.; Yoshida, H.; Satsuma, A.; Tanaka, T.; Yoshida, S.; Hattori, T. *J. Phys. Chem. B* **1998**, *102*, 10190–10195.
(28) Erker, G.; Albrecht, M.; Krueger, C.; Werner, S. *J. Am. Chem. Soc.* **1992**, *114*, 8531–8536.
(29) William, J. E.; Reiner, A.; Robert, J. D.; Joseph, W. Z. *Angew. Chem., Int. Ed.* **1994**, *33*, 1641–1644.
(30) Basharat, S.; Betchley, W.; Carmalt, C. J.; Barnett, S.; Tocher, D. A.; Davies, H. O. *Organometallics* **2006**, *26*, 403–407.
(31) Faro Júnior, A. C.; Eon, J. G.; Nogueira, L.; da Silva, R. F.; Rodrigues, V. O. *Catal. Today* **2008**, *133*−*135*, 913–918.
(32) Stern, E. A. *Phys. Rev. B* **1993**, *48*, 9825.
(33) Smith, M. B. *J. Organomet. Chem.* **1972**, *46*, 31–49.
(34) Coates, G. E.; Downs, A. J. *J. Chem. Soc.* **1964**, 3353–3356.
(35) Beagley, B.; Schmidling, D. G. *J. Mol. Struct.* **1974**, *21*, 437–444.
(36) Muñoz, M.; Argoul, P.; Farges, F. *Am. Mineral.* **2003**, *88* 694–700.
(37) Funke, H.; Scheinost, A. C.; Chukalina, M. *Phys. Rev. B* **2005**, *71*, 094110.
(38) Persson, P.; Zivkovic, K.; Sjoberg, S. *Langmuir* **2006**, *22* 2096–2104.
(39) Savinelli, R. O.; Scott, S. L. *Phys. Chem. Chem. Phys.* **2010**, *12*, 5660–5667.
(40) Bunker, B. C.; Haaland, D. M.; Michalske, T. A.; Smith, W. L. *Surf. Sci.* **1989**, *222*, 95–118.
(41) Morrow, B. A.; Gay, I. D. *J. Phys. Chem.* **1988**, *92*, 5569–5571.
(42) Chuang, I. S.; Maciel, G. E. *J. Phys. Chem. B* **1997**, *101* 3052–3064.
(43) Uhl, W.; Hannemann, F. *J. Organomet. Chem.* **1999**, *579*, 18–23.
(44) Veith, M.; Vogelgesang, H.; Huch, V. *Organometallics* **2001**, *21*, 380–388.
(45) Prager, M.; Combet, J.; Parker, S. F.; Desmedt, A.; Lechner, R. E. *J. Phys.: Condens. Matter* **2002**, *14*, 10145–10157.
(46) Hill, R. J.; Gibbs, G. V. *Acta Crystallogr. Sect. B: Struct. Sci.* **1979**, *35*, 25–30.
(47) Lasaga, A.; Gibbs, G. *Phys. Chem. Miner.* **1987**, *14*, 107–117.
(48) Peglar, R. J.; Hambleton, F. H.; Hockey, J. A. *J. Catal.* **1971**, *20*, 309–320.
(49) Morrow, B. A.; McFarlane, R. A. *J. Phys. Chem.* **1986**, *90* 3192–3197.
(50) Almond, M. J.; Jenkins, C. E.; Rice, D. A.; Hagen, K. *J. Organomet. Chem.* **1992**, *439*, 251–261.
(51) Koide, Y.; Bott, S. G.; Barron, A. R. *Organometallics* **1996**, *15*, 5514–5518.
(52) Avnir, D.; Farin, D.; Pfeifer, P. *J. Chem. Phys.* **1983**, *79* 3566–3571.
(53) Rojanski, D.; Huppert, D.; Bale, H. D.; Dacai, X.; Schmidt, P. W.; Farin, D.; Seri-Levy, A.; Avnir, D. *Phys. Rev. Lett.* **1986**, *56*, 2505.
(54) Bakos, T.; Rashkeev, S. N.; Pantelides, S. T. *Phys. Rev. B* **2004**, *69*, 195206.
(55) Ravel, B.; Newville, M. *J. Synchrotron Radiat.* **2005**, *12*, 537–541.
(56) Ankudinov, A. L.; Ravel, B.; Rehr, J. J.; Conradson, S. D. *Phys. Rev. B* **1998**, *58*, 7565.
(57) Rice, G. L.; Scott, S. L. *Langmuir* **1997**, *13*, 1545–1551.
(58) Frisch, M. J.; et al. *Gaussian 03*, Revision C.02; Gaussian, Inc.: Wallingford, CT, 2004.
(59) Lee, C.; Yang, W.; Parr, R. G. *Phys. Rev. B* **1988**, *37*, 785.
(60) Becke, A. D. *Phys. Rev. A* **1988**, *38*, 3098.